Journal of Soils and Sediments (2020) 20:911–920
https://doi.org/10.1007/s11368-019-02444-x

SOILS, SEC 4 • ECOTOXICOLOGY • RESEARCH ARTICLE

Effect of humic acid on the sedimentation and transport of nanoparticles silica in water-saturated porous media

Mo Zhang[1] · Duo Li[1] · Zhi Ye[1] · Shiqi Wang[1] · Nan Xu[1] · Fang Wang[1] · Shouqing Liu[1] · Jianping Chen[2] · Huajie Gu[1]

Received: 2 July 2019 / Accepted: 27 August 2019 / Published online: 4 September 2019

Abstract

Purpose Nano silicon particles ($nSiO_2$) is one of the most widely used industrial engineered nanomaterials (ENMs). The extensive applications of $nSiO_2$ may pose potential risks to aquatic ecosystems and human health. Humic acid (HA) is a major component of soil and water that exists widely in the natural environment and adsorbs to the surface of nanoparticles, which affects the fate and transport of ENMs in soil. Therefore, it triggers the necessity to study the chemical reaction of HA controlling the sedimentation and transport of $nSiO_2$.

Materials and methods The sedimentation kinetics and transport breakthrough curves of $nSiO_2$ with/without HA in water-saturated porous media were studied in two electrolyte (NaCl and $CaCl_2$) solutions. The likely mechanisms were explored with both multiple technologies and numerical modeling including TEM-EDX, particle size distribution, zeta potentials, and the two-site kinetic attachment model (TSKAM).

Results and discussion Our experimental results showed that the existence of HA generally increased the suspensivity and the transportability of $nSiO_2$ in NaCl and $CaCl_2$ solutions in packed sand columns at acidic pH. This result was attributed to the HA adsorption leading to the more negatively charged surface and the smaller size of $nSiO_2$ aggregates. However, the formation of coordination complexes associated with larger cluster among $nSiO_2$ between HA and Ca^{2+} contributed to the increased sedimentation of $nSiO_2$ at alkaline pH. Subsequently, the presence of HA inhibited the transport of $nSiO_2$ in $CaCl_2$ solution at pH 9.0. Comparably, in NaCl at pH 9.0, HA showed the negligible effect on the $nSiO_2$ deposition in sand. Both the attachment and detachment parameters, which were obtained from fitting the breakthrough curves of ENMs using the TSKAM, could be used to well describe the transport behavior of $nSiO_2$ with HA under various conditions. In particular, the irreversible attachment parameters at site 2 on sand were positively related to the retention of $nSiO_2$ with HA.

Conclusions The fate and transport of $nSiO_2$ can be distinctly affected by HA depending on the ion composition, ion strength, and pH in soil. This study will provide insights for assessing the mobility of $nSiO_2$ with HA in subsurface soil and aquatic environments.

Keywords Humic acid (HA) · Modeling · Nano silicon particles ($nSiO_2$) · Particle size · Transport

Responsible editor: Dong-Mei Zhou

Electronic supplementary material The online version of this article (https://doi.org/10.1007/s11368-019-02444-x) contains supplementary material, which is available to authorized users.

✉ Nan Xu
nanxu@mail.usts.edu.cn

[1] Jiangsu Key Laboratory of Environmental Functional Materials, School of Chemistry Biology and Material Engineering, Suzhou University of Science and Technology, Suzhou 215009, China

[2] Jiangsu Key Laboratory of Intelligent Building Energy Efficiency, Suzhou University of Science and Technology, Suzhou 215009, China

1 Introduction

With a rapid development in the nanotechnology industry, there are increasing concerns about the production and application of engineered nanomaterials (ENMs) (USEPA, 2007). Nano silica ($nSiO_2$), as one of industrial inorganic ENMs, are widely used in various fields like paint (Diener et al. 2013), rubber (Cochrane and Lin 1993), plastics (Cho and Sul 2001), pigments (Yuan et al. 2008), biology, and medicine (Li et al. 2012). It is inevitably released into the soil and water environments during process and usage which result in the potential hazard to human health and environment (Oberdörster et al. 1994; Adams et al. 2006; Nel et al. 2006). Some studies have been carried out on the toxic

effects of $nSiO_2$ on animals, microorganisms, plants, and human being cells (Fruijtier-Polloth 2012). Although, there is no evidence from limited animal studies that $nSiO_2$ induce reproductive or developmental toxicity. $nSiO_2$ may enter the body in particulate or dissolved form, which depended on aggregate size of silica particles and pH (Cho et al. 2009). Also, the $nSiO_2$ pose potential hazards to human by penetrating the intracellular targets in the lung and systemic circulation (Napierska et al. 2010).

Because these ENMs could be released into the environment during application or transportation, more and more researchers are paying attention to the fate and transport of ENMs. The mutual electrostatic reactions between receptors and ENMs may result in the difference in deposition of ENMs (Jiang et al. 2010; Li et al. 2012), which were affected by many factors in natural environment: ionic species, ionic strength (Solovitch et al. 2010), bacteria, pH, surfactant, and organic matter. Except that, the surface roughness of soil (Redman et al. 2001), charge heterogeneity of ENMs (Johnson and Elimelech 1995), and variability in the characteristics of colloid (Bolster et al. 1999) contributed to the different retention of ENMs in soil. As a kind of natural organic matter (NOM), humic acid (HA) is formed by complex biochemical reactions of animals and plants debris which present in the groundwater and soil environments. HA is consist of large amount of carboxylic and phenolic functional groups (Amirbahman and Olson 1995). Therefore, HA adsorption can alter the ENMs surface properties, and consequently impacts their transport patterns: nanoparticle zero-valent iron (nZVI) (Johnson et al. 2009), fullerenes (Espinasse et al. 2007; Loon and Menachem 2008), titanium oxide (TiO_2) (Ben-Moshe et al. 2010; Doshi et al. 2008; Fisher-Power and Cheng 2018; Chen et al. 2018), zinc oxide (ZnO) (Jiang et al. 2010), natural colloids (clays) (Kretzschmar et al. 1999; Hahn and O'meliae 2004), biochar (Wang et al. 2013), and hydroxyapatite nanoparticles (Wang et al. 2012b). For instance, NOM showed distinct effects on the transport behavior of rutile TiO_2 in quartz sands (Chen et al. 2012). NOM was found to facilitate the transport of rutile TiO_2 at low pH but have no effect under alkaline condition. The combined factors of HA and bacteria favor the transport of $nTiO_2$ (Guggenberger et al. 2008). Additionally, HA also could facilitate the transportability of bare nZVI (Jung et al. 2014). As known, the distinct physicochemical properties of ENMs and the subtly different compositions of soil and water contributed to the different transport behavior (Bayat et al. 2015). Currently, the particle size and phosphate have been reported to influent the $nSiO_2$ transport in water-saturated porous sand (Wang et al. 2012a; Liu et al. 2017). However, there is li information available on the mobility or transport behavior of $nSiO_2$ with HA.

In this study, the HA effect on the sedimentation and transport of $nSiO_2$ in the water-saturated sand medium were researched in monovalent (Na^+) and divalent (Ca^{2+}) electrolyte solutions. Besides, the zeta potentials and hydrodynamic radius of $nSiO_2$ with HA were measured correspondingly. The underlying mechanism controlling the transport behavior of $nSiO_2$ with HA was described using a two-site kinetic attachment model (TSKAM) to imitate their breakthrough curves (BTCs) in sand porous media.

2 Materials and methods

2.1 Preparation of $nSiO_2$ suspension

The $nSiO_2$ with a purity of 99.9 % is obtained from the Aladdin Reagent Company. The $nSiO_2$ samples characterized by powder X-ray diffraction (XRD, D8-Focus, Bruker AXS Co., Ltd., Germany) are spherical particles. The particle size of $nSiO_2$ was ~ 15 × 20 nm, which was the mean values based on the measurements from five different locations performed using transmission electron microscopy (TEM, FEI Tecnai G2 F20 S-Twin, USA). Its characteristic surface area was 200 $m^2\ g^{-1}$, which was estimated by a nitrogen multi-point BET isotherm.

Before transport experiments, 50 mg L^{-1} $nSiO_2$ suspension was prepared in NaCl or $CaCl_2$ electrolyte solution containing different HA (purchased from Sigma-Aldrich company) concentrations (0–3 mg L^{-1}) at certain pH. The tested $nSiO_2$ and HA concentrations were consistent with those reported in the literature (Redman et al. 2002; Chen et al. 2012; Chowdhury et al. 2012; Wang et al. 2012a, b). Previous researchers used pH as high as 10.0 in order to minimize surface charge heterogeneity and also to ensure attachment of silica nanoparticles under unfavorable conditions (Bradford et al. 2009; Zhang et al. 2010; Wang et al. 2012a). Thus, the pH values of 6.0 and 9.0 were chosen in this study, which were consistent with other studies on ENMs transport in the presence of HA (Chen et al. 2012; Wang et al. 2012b). And then the $nSiO_2$ suspensions were homogenized by a magnetic stirrer for 1 min and sonicated for another 30 min for better dispersivity. In addition, all the chemical reagents (AR) used in this study were obtained from the Chinese medicine group.

2.2 Measurements of zeta potentials and hydraulic radius

A set of $nSiO_2$ (50 mg L^{-1}) suspensions with or without HA (1 and 3 mg L^{-1}) in electrolyte solutions were adjusted to pH values of 6.0 and 9.0 using a diluted HCl or NaOH solution. Then, samples were sonicated for 30 min before further analysis. Finally, a Zeta-sizer Nano ZS90 (Malvern Instruments Ltd., Malvern, UK) was employed to exam the hydrodynamic radius of particles and the dynamic light scattering (DLS) measurement was used to determine their zeta potential at room temperature.

2.3 Sedimentation experiments

Sedimentation experiments were conducted to investigate the dynamics of the aggregation process using a spectrophotometer

(UV-2450, Shimadzu Scientific Instrument, Japan). Briefly, after ultrasonication for 30 min, the suspensions of $nSiO_2$ with or without HA were placed in a cuvette of spectrophotometer. The samples were read at 5-min intervals over 2 h and the concentration of $nSiO_2$ in cuvette was directly determined using a UV-Vis spectrophotometer based on pre-established calibration curves (Fig. S1a, Electronic Supplementary Material - ESM) in supporting information (SI) at 250 nm, where HA show almost no adsorption effect on detection of $nSiO_2$ (Fig. S1b - ESM). Sedimentation curve was analyzed by calculating the concentration ratio (C/C_0) of $nSiO_2$ as a function of time, in which C_0 and C are the concentrations of SiO_2 at initial and the certain time of sedimentation, respectively. Supposed that no dissolution of the $nSiO_2$ happened in any of the solutions. Thus, any decrease in $nSiO_2$ concentration over time was on the account of sedimentation.

2.4 Column transport experiments

Quartz sand used in all the transport experiments was pretreated (Chen et al. 2015). Glass chromatography columns (2.5 cm inner diameter and 20 cm long) were filled evenly with the pretreated quartz sands as the porous media, which were covered with the 80-μm nylon net film at both ends. Once filled, the columns were saturated with deionized water for more than 24 h. The procedural details were mentioned in previous studies (Xu et al. 2017). Briefly, 4 pore volumes (PVs) of electrolyte solution was pumped upward to columns at a constant flow rate (1 mL min^{-1}). It has been reported that the addition of HA in the presence of Ca^{2+} resulted in decreased critical coagulation concentration of silicon nanoparticles from 0.4 to 0.1 M (Liu et al. 2011). Therefore, 100–300 mM NaCl or $CaCl_2$ were used as electrolyte solutions in this study. Then, another 4 PVs of particle suspension which was homogenized by a magnetic stirrer at the same time, was introduced at the same flow rate (phase I). After that, 4 PVs of electrolyte solution was pumped toward columns during phase II and 4 PVs of deionized water was flushed as well until no $nSiO_2$ detected in column effluents during phase III. Finally, the breakthrough curves (BTCs) of C/C_0 (where the concentrations of $nSiO_2$ in influent (C_0) and effluent (C) passing through columns) were determined as a function of PV. The corresponding physical parameters for transport experiments were summarized and presented in Table S1 (see ESM). The Si analysis was based on the silicon molybdenum yellow method by colorimetry (Liu et al. 2017).

2.5 Modeling

The mass transfer of ENMs between the aqueous and solid phases has been successfully described using an improved form of the advection-dispersion equation (ADE) and the TSKAM (Bradford et al. 2003; Schijven and ŠimŮnek 2002). Currently, there is little information available on describing the transport behavior of $nSiO_2$ with HA in porous media using TSKAM. In this work, TSKAM was used to simulate the breakthrough curves (BTCs) of $nSiO_2$ with HA in water-saturated sand using the HYDRUS-1D code (Simunek et al. 2016), which used a nonlinear least-squares optimization routine based on the Levenberg-Marquardt algorithm to fit $nSiO_2$ transport parameters (Chen et al. 2015; Esfahani et al. 2014; Xu et al. 2018). The corresponding equations are defined in text in the SI.

3 Results and discussion

3.1 Zeta potential of $nSiO_2$ with and without HA

The zeta potential (ZP) of NPs is a significant influence factor for particle aggregation or stability in solution. As the representative, NaCl and $CaCl_2$ electrolyte solutions were chosen to investigate the zeta potentials of $nSiO_2$ with HA at certain pH values (6.0 and 9.0). The surface charges of $nSiO_2$ became less negative as increasing the ion concentration (IC) of electrolyte because of the charge shielding effect and the compression of the surface double layer. In NaCl, the $nSiO_2$ surface was more negatively charged as the HA concentration increased (Fig. 1a, b). Specifically, the ZP of $nSiO_2$ in 200 mM NaCl solution was − 13.93 mV in the absence of HA and − 17.87 mV in the presence of 3 mg L^{-1} HA at pH 6.0. The ZPs at pH 9.0 (Fig. 1b) were more negative than that at pH 6.0 (Fig. 1a). It attributed to that a larger charge density was formed on the surface of $nSiO_2$ after deprotonation of surface hydroxyl (Svecova et al. 2008) under the alkaline pH. Furthermore, the ZPs of $nSiO_2$ were negligibly changed with the increase of HA, due to subtle adsorption of HA at high pH.

Considering the specific absorption occurred which refers to the Ca^{2+} adsorption on the surface (Schulman 1960), the individual $nSiO_2$ surface became more positive in $CaCl_2$ (Fig. 1c–d) than that in NaCl at the same pH (Fig. 1a–b). In the presence of HA, the negative charge on the $nSiO_2$ surface increased (Fig. 1c–d), since Ca^{2+} adsorbed to the surface of $nSiO_2$ can react with HA to form coordination complexes (Liu et al. 2011).

3.2 Sedimentation kinetics of $nSiO_2$ with and without HA

The sedimentation kinetics of $nSiO_2$ with/without HA were investigated in Na^+ and Ca^{2+} solutions at pH 6.0 and 9.0 (Fig. 2). In 300 mM NaCl solutions at pH 6.0, the percentage normalized concentration (C/C_0) of $nSiO_2$ without HA dropped down quickly in the first 30 min and then remained 38 % for 2 h. With the addition of 1 mg L^{-1} HA, the C/C_0 (45 %) increased slightly and presented a little better stability

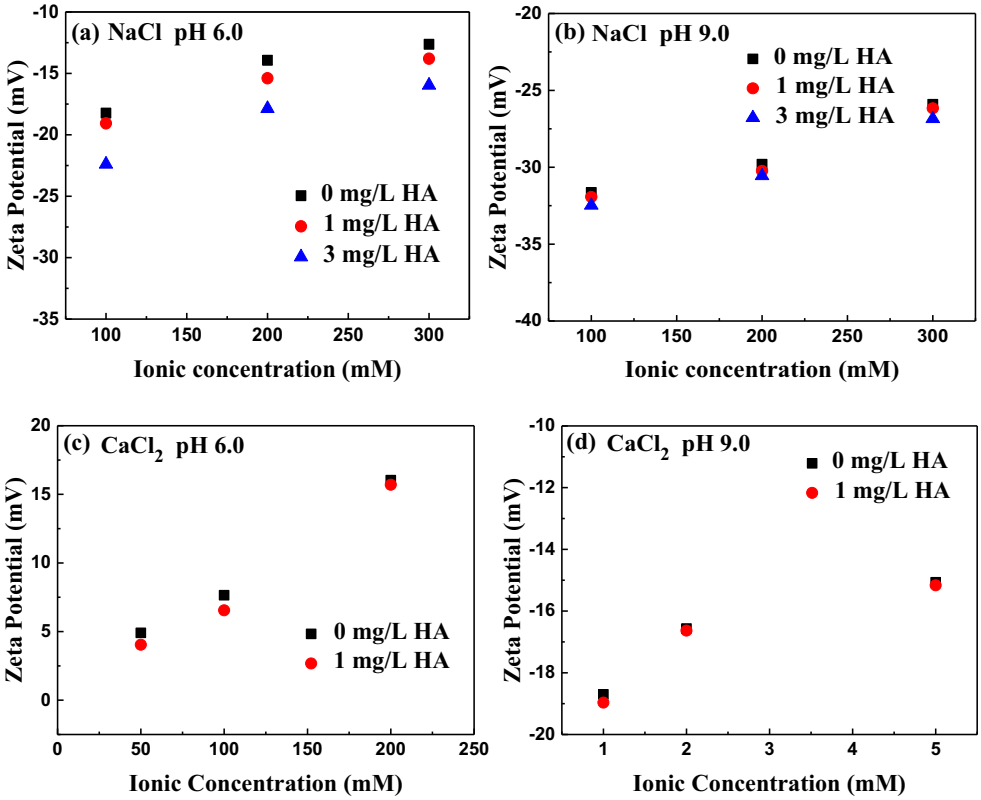

Fig. 1 Zeta potentials of $nSiO_2$ with and without humic acid (HA) as a function of ion concentration in NaCl (**a**, **b**) and in $CaCl_2$ (**c**, **d**) solutions at pH 6.0 (**a**, **c**) and 9.0 (**b**, **d**)

compared to individual $nSiO_2$ (Fig. 2a). This was because of the stronger electrostatic repulsion due to the more negatively charged surface with the increase in HA (Fig. 1a). As a result, the particle size decreased gradually with increasing the HA as

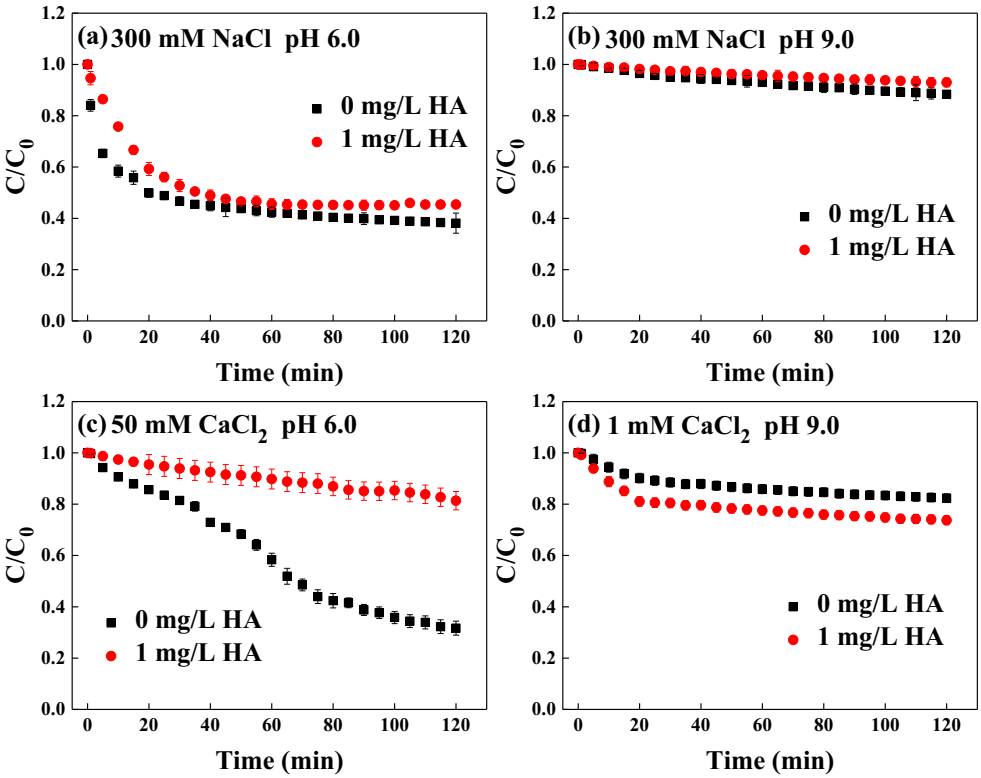

Fig. 2 Sedimentation kinetics of $nSiO_2$ with 1 mg L^{-1} and without humic acid (HA) in 300 mM NaCl (**a**, **b**), 50 mM $CaCl_2$ (**c**) and 1 mM $CaCl_2$ (**d**) solutions at pH 6.0 (**a**, **c**) and 9.0 (**b**, **d**)

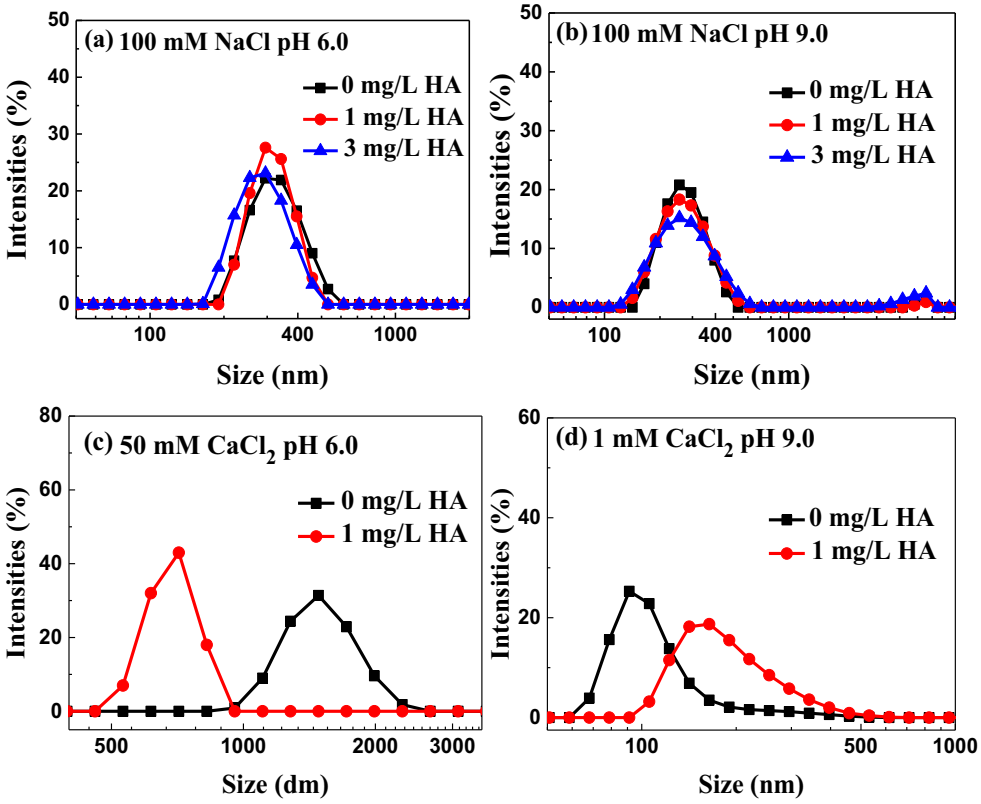

Fig. 3 Size distributions of $nSiO_2$ with and without humic acid (HA) in 100 mM NaCl (**a**, **b**), 50 mM $CaCl_2$ (**c**) and 1 mM $CaCl_2$ (**d**) solutions for influents of column experiments at pH 6.0 (**a**, **c**) and 9.0 (**b**, **d**)

the intensity-weighted particle size distribution in NaCl at pH 6.0 shown in Fig. 3a. When pH increased from 6.0 to 9.0, the stability of $nSiO_2$ with and without HA was significantly improved (Fig. 2b vs. Fig. 2a). It might be due to the more negatively charged at pH 9.0 (Fig. 1b) than that at pH 6.0 (Fig. 1a). HA had subtle effects on the stability of $nSiO_2$ in NaCl solution. As supported, the particle size distribution showed negligible change (Fig. 3b), due to the subtle absorption of HA onto $nSiO_2$.

Notably, in 50 mM $CaCl_2$ solution at pH 6.0, HA significantly improved the dispersivity of $nSiO_2$ suspension (Fig. 2c). In detailed, the individual $nSiO_2$ continuously

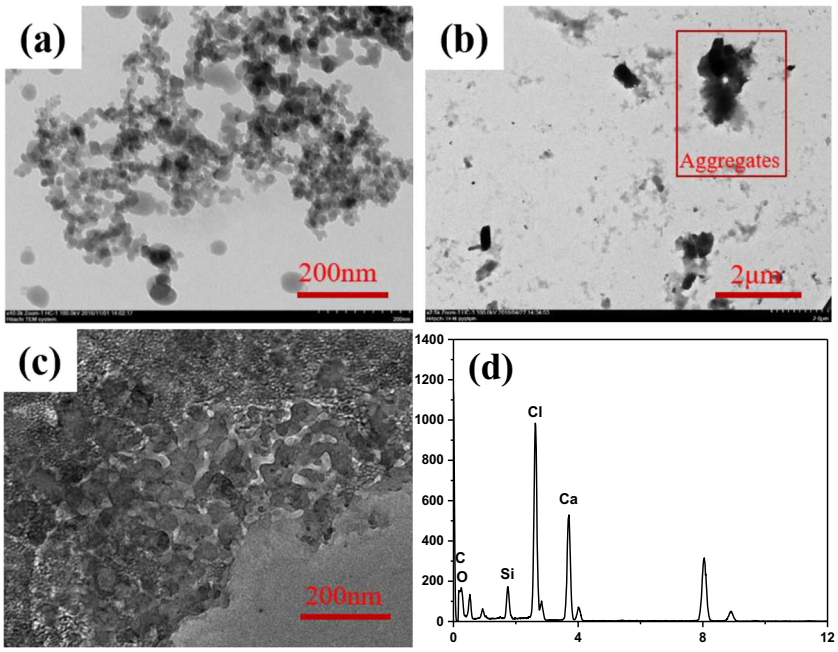

Fig. 4 TEM images of individual $nSiO_2$ suspended in NaCl solution (**a**) and $nSiO_2$ with humic acid (HA) in $CaCl_2$ solution (**b**, **c**), and the corresponding EDX spectra (**d**) in $CaCl_2$ solution

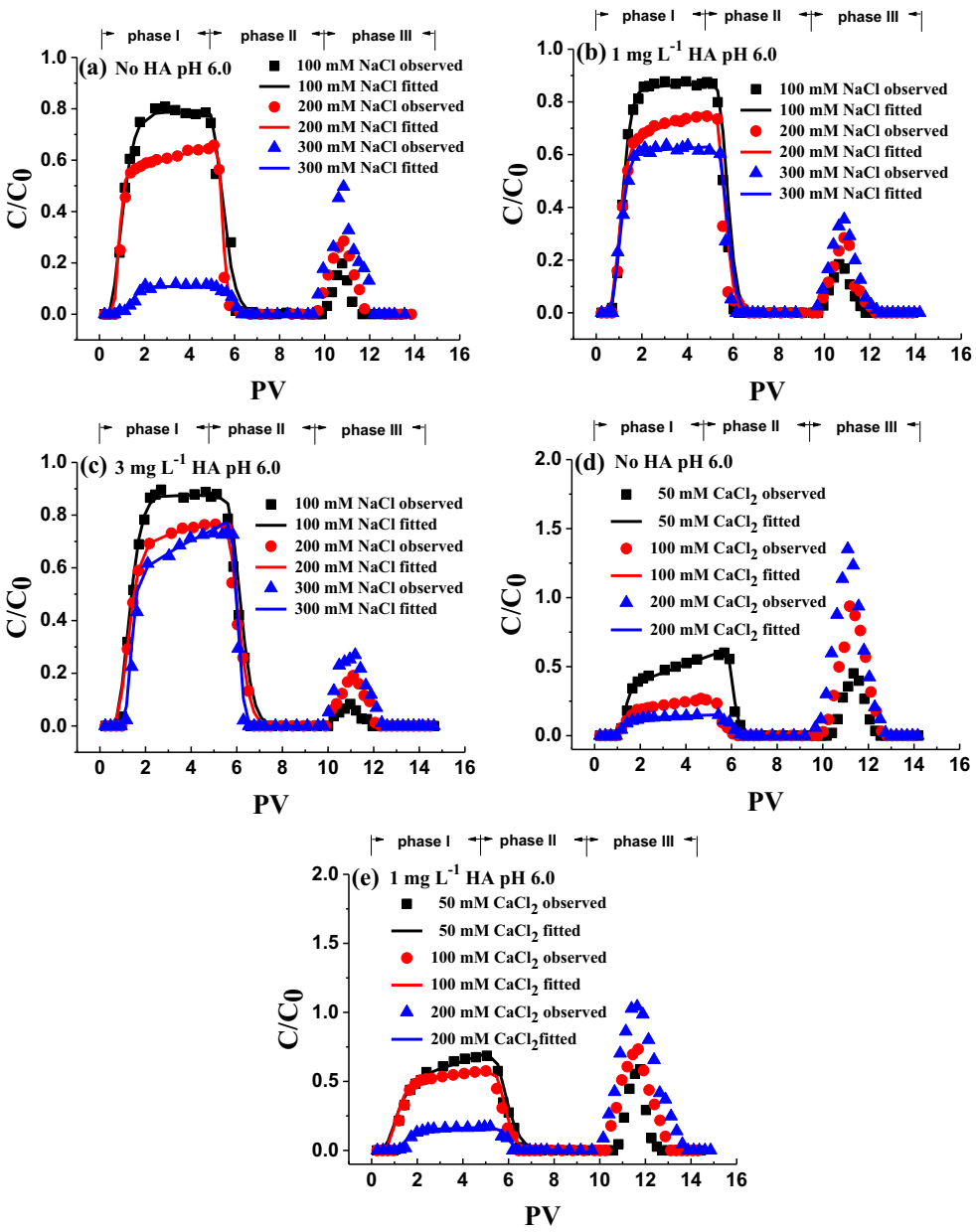

Fig. 5 Breakthrough curves of $nSiO_2$ with the absence (**a**) and presence of 1 mg L^{-1} (**b**) and 3 mg L^{-1} (**c**) humic acid (HA) in NaCl electrolyte, and with the absence (**d**) and the presence of 1 mg L^{-1} (**e**) HA in $CaCl_2$ electrolyte at pH 6.0

settled down and only 30 % of $nSiO_2$ remained in suspension. However, this value increased to 80 % finally with the addition of HA, which was contributed to slightly lower absolute values of surface charge (Fig. 1c). This result was consistent with the smaller sizes of particles with HA as shown in Fig. 3c. For instance, the size of individual $nSiO_2$ in 50 mM $CaCl_2$ was mainly distributed around 1484 nm, whereas that was around 712 nm after addition of 1 mg L^{-1} HA. Conversely, HA did inhibit the dispersion of $nSiO_2$ in 1 mM $CaCl_2$ at pH 9.0. As shown in Fig. 2d, about 82 % of individual $nSiO_2$ remained stable in suspension, whereas C/C_0 of $nSiO_2$ decreased to 73 % with the addition of HA. At pH 9.0, the individual $nSiO_2$ in 1 mM $CaCl_2$ was mainly around 90 nm, while the particles size was distributed at 160 nm after the HA present in solution (Fig. 3d). This result appeared the HA increased the size of $nSiO_2$ in Ca^{2+} solution at alkaline pH, which can be supported by the formation of larger coordination complexes among $nSiO_2$ by a bridge between HA and Ca^{2+} (Liu et al. 2011). In order to verify this, TEM images were taken to show that the regular nanoparticles of SiO_2 were relatively distributed in NaCl solution after HA was added (Fig. 4a). Nevertheless, with the addition of HA, the large aggregates were formed in Ca^{2+} solution (Fig. 4b). These aggregates were composed of the agglomerated nanoparticles with unclear and irregular surface (Fig. 4c), which were consisted of Si, O, and Ca elements (Fig. 4d). This result suggested that large $nSiO_2$ aggregates were formed with interplay between HA and Ca^{2+}.

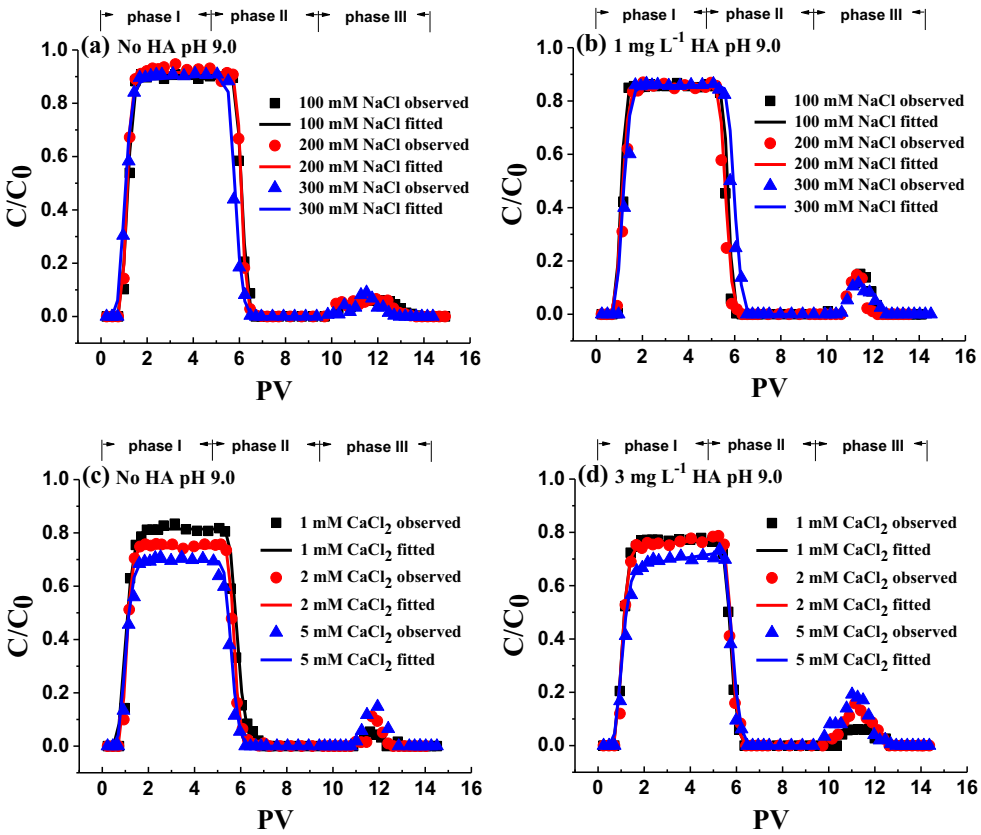

Fig. 6 Breakthrough curves of $nSiO_2$ with the absence (**a**) and presence of 1 mg L^{-1} (**b**) humic acid (HA) in NaCl electrolyte, and with the absence (**c**) and the presence of 1 mg L^{-1} HA (**d**) in $CaCl_2$ electrolyte at pH 9.0

3.3 Transport of $nSiO_2$ with and without HA

The BTCs of $nSiO_2$ with and without HA in packed quartz sands simulated by a TSKAM were shown in Figs. 5 and 6, and the related model parameters were concluded in Table 1 under various experimental conditions. Note that the R^2 values obtained from fitting the models were all greater than 0.97, which suggested that the model showed a good simulation in the $nSiO_2$ transport in the presence of HA.

Generally, the transport parameters (k_1, k_{1d}, k_2) from TSKAM were first-order coefficients [T^{-1}]. It was shown in Table 1 that the irreversible straining coefficient (k_2) at site 2 on sand is obviously less than the reversible attachment and detachment coefficients (k_1 and k_{1d}) at site 1 in all experiments. This implied that the retention of $nSiO_2$ was reversible during phase I and II. As expected, $nSiO_2$ could be detected in effluent during phase III regardless the existence of HA (Figs. 5 and 6). Furthermore, the values of k_1 were clearly greater than those of k_{1d}, even though the k_1 had a magnitude similar to k_{1d}. As a result, the values of k_{1d}/k_1 were lower than 1 for $nSiO_2$ with and without HA. It indicated that the attachment interaction between $nSiO_2$ (with or without HA) and quartz sand was stronger than the detachment. It was consistent with the transport behavior of silver (Liang et al. 2013) and zinc oxide (Zhu et al. 2005) NPs in soil. Noted that the k_{1d}/k_1 values for $nSiO_2$ with HA in NaCl and $CaCl_2$ solutions were more than that without HA at pH 6.0 (Table 1). Accordingly, the transport of $nSiO_2$ was facilitated by the addition of HA under acidic condition (Fig. 5a vs. b and d vs. e), which was consistent with the facilitated transport of hydroxyapatite by HA (Wang et al. 2012b). However, the different phenomenon was observed at pH 9.0. Especially, in NaCl solution, the k_{1d}/k_1 values for $nSiO_2$ with HA were almost similar as those without HA at pH 9.0 (Table 1), which was consistent with the negligible difference between $nSiO_2$ with and without HA (Fig. 6a vs. b). This was possibly because HA showed an insignificant effect on the stability (Fig. 2b) and particle size of $nSiO_2$ (Fig. 3b) in Na^+ solution at pH 9.0, due to low adsorption of HA on SiO_2. This result was consistent with slight change in zeta potentials of $nSiO_2$ after HA was added in NaCl solution at pH 9.0 (Fig. 1c). In $CaCl_2$ at pH 9.0, the k_{1d}/k_1 values for $nSiO_2$ with HA were less than those without HA (Table 1). This suggested that the detachment at site 1 on sand was decreased by the presence of HA. As previously discussed, the larger coordination complexes among $nSiO_2$ by a bridge of HA-Ca^{2+} (Liu et al. 2011) might contribute to the increased deposition of $nSiO_2$ with HA in sand at alkaline pH (Fig. 6c vs. d).

In addition, high pH decreased the values of k_2 regardless of the HA existence. For example, with the increase in NaCl (100–300 mM), the k_2 value for $nSiO_2$ with 1 mg L^{-1} HA was in the range of 0.007~0.022 min^{-1} and 0.006~0.009 min^{-1} at

Table 1 Fitted parameters of the TSKAM as estimated from the breakthrough data for packed quartz sands under different experimental conditions

IC (mM)	HA[c] (mg L^{-1})	pH	k_1[d] (min^{-1})	k_{1d}[e] (min^{-1})	k_{1d}/k_1	k_2[f] (min^{-1})	R^2[g]	MR_{12}[h] (%)	MR_3[i] (%)
100[a]	0	6.0	0.199	0.168	0.844	0.011	0.989	81.27	12.0
200[a]	0	6.0	0.868	0.478	0.551	0.027	0.999	60.21	14.98
300[a]	0	6.0	1.284	0.631	0.491	0.042	0.976	11.46	27.39
100[a]	1	6.0	0.525	0.474	0.903	0.007	0.987	88.78	9.75
200[a]	1	6.0	0.430	0.359	0.835	0.020	0.985	73.17	13.58
300[a]	1	6.0	0.332	0.249	0.750	0.022	0.985	62.56	17.43
100[a]	3	6.0	0.599	0.555	0.927	0.009	0.990	85.82	4.81
200[a]	3	6.0	0.433	0.383	0.885	0.016	0.993	75.31	11.08
300[a]	3	6.0	0.365	0.308	0.844	0.023	0.993	74.14	16.83
50[b]	0	6.0	0.140	0.081	0.579	0.046	0.993	50.25	20.16
100[b]	0	6.0	0.404	0.201	0.498	0.077	0.995	22.19	42.54
200[b]	0	6.0	0.724	0.259	0.358	0.096	0.994	10.21	61.22
50[b]	1	6.0	0.033	0.021	0.636	0.033	0.982	60.86	28.34
100[b]	1	6.0	0.158	0.088	0.557	0.042	0.982	55.42	42.18
200[b]	1	6.0	0.533	0.254	0.477	0.087	0.973	15.33	50.55
100[a]	0	9.0	1.469	1.360	0.926	0.005	0.993	86.88	4.43
200[a]	0	9.0	3.368	3.250	0.965	0.006	0.998	89.83	3.64
300[a]	0	9.0	5.660	5.280	0.932	0.009	0.994	87.92	3.66
100[a]	1	9.0	1.138	0.925	0.913	0.006	0.991	86.26	7.75
200[a]	1	9.0	0.970	0.819	0.944	0.008	0.987	85.82	8.43
300[a]	1	9.0	0.405	0.330	0.915	0.009	0.987	88.99	6.39
1[b]	0	9.0	0.566	0.534	0.943	0.012	0.989	79.34	2.22
2[b]	0	9.0	0.821	0.779	0.949	0.013	0.999	77.62	3.85
5[b]	0	9.0	1.513	1.435	0.948	0.016	0.995	72.75	6.51
1[b]	1	9.0	2.330	2.123	0.911	0.015	0.989	81.24	4.53
2[b]	1	9.0	0.906	0.804	0.887	0.017	0.994	72.87	8.93
5[b]	1	9.0	0.563	0.501	0.890	0.018	0.993	68.22	9.50

[a] Concentration of the NaCl electrolyte solutions

[b] Concentration of the $CaCl_2$ electrolyte solutions

[c] Initial HA concentration injected into the saturated sand columns

[d] First-order attachment coefficient on site 1

[e] First-order detachment coefficient on site 1

[f] First-order retention coefficient on site 2

[g] Squared Person's correlation coefficient

[h] The mass recovery of phase I and phase II

[i] The mass recovery of phase III

pH 6.0 and 9.0 (Table 1), respectively. It was also consistent with the variation of k_{1d}/k_1. It indicated the straining process of $nSiO_2$ at site 2 on sand decreased. The reason could be that the hydrodynamic size became larger as the pH decreased in NaCl (Fig. 3a vs. b). In $CaCl_2$ solution, zeta potential experimental results suggested that the surfaces of $nSiO_2$ with and without HA were positively charged at pH 6.0 and negatively charged at pH 9.0 (Fig. 1c vs. d). In contrast, quartz sand was usually negatively charged (Liu et al. 2017). The charge heterogeneity resulted in an increase of straining at site 2 at pH 6.0 compared to that at pH 9.0. This increased the irreversible attachment interaction of $nSiO_2$ in $CaCl_2$ at pH 6.0. As a result, the low pH favors the deposition of $nSiO_2$ independent of HA.

Given that values of k_1 and k_2 for individual $nSiO_2$ increased with increasing the IS (Table 1). This suggested that the greater retention of $nSiO_2$ was related to the depth of the secondary minimum (Toloni et al. 2014; Tufenkji and Elimelech 2005). However, the different change trend of parameters took place after the addition of HA: k_1 decreased and k_2 increased with increasing the IS. Also noted, k_2 with HA was less than that without HA under the same conditions. For example, the k_2 for individual $nSiO_2$ increased from 0.011 to 0.042 min^{-1} with

the increase of Na^+ at pH 6.0, while that with the HA ranged from 0.007 to 0.022 min^{-1} (Table 1). This result was consistent with the facilitated transport of nSO_2 with HA due to the decreased irreversible retention resulting from HA adsorption (Fig. 5a vs. c and d vs. e). However, in Ca^{2+} at pH 9.0, k_1 with HA was greater than that without HA, which was again due to the formation of larger coordination complexes among $nSiO_2$ by a bridge between HA and Ca^{2+} (Liu et al. 2011). As supported, the value of k_2 was slightly increased by the presence of HA at alkaline pH (Table 1). This indicated that the HA increased the irreversible deposition of $nSiO_2$ in $CaCl_2$ solution at pH 9.0 (Fig. 6c vs. d). To elucidate the direct influence of HA on the transport of $nSiO_2$ in soils containing calcium, additional experiment was conducted: HA was injected to the SiO_2 and Ca^{2+} pre-deposited sand column at pH 9.0. The breakthrough curves (BTCs) of particulate $nSiO_2$ was presented in Fig. S2 (ESM). The shape of the BTCs for $nSiO_2$ in phases I and II was similar to that for individual $nSiO_2$ in $CaCl_2$ at pH 9.0 (Fig. 6c). However, a certain amount of $nSiO_2$ with HA in $CaCl_2$ influent was flushed out from sand column by DI water during phase III (Fig. 6d). However, almost no $nSiO_2$ with HA could be detected during phase III (Fig. S2 - ESM). This result demonstrated that the pre-deposited $nSiO_2$ in sand was irreversible, which was difficult to leach from sand column, but prone to deposition by the formation of larger complexes between HA and Ca^{2+}.

4 Conclusions

The sediment and transport behavior of $nSiO_2$ with HA in porous media was investigated in the system. The impacts of IC, HA concentration, and pH were studied in great detail. HA could adsorb to the surface of $nSiO_2$, which lead to the more negatively charged surface and smaller particle size of $nSiO_2$, thus improved the suspension stability of $nSiO_2$ and facilitated their transport in NaCl and $CaCl_2$ at acidic pH. This effect was strengthened with the increase of HA level. However, HA can form coordination complexes with calcium ions which adsorbed to the $nSiO_2$ surface in $CaCl_2$ electrolyte at alkaline pH and resulted in the larger complexes, thus increased the sedimentation rate and inhibited the transport of $nSiO_2$. Particularly, due to the specific absorption occurred between Ca^{2+} and $nSiO_2$, the surface of $nSiO_2$ was positively charged at larger calcium concentrations. The two-site kinetic attachment model fitting results showed that the combined values of the attachment/detachment coefficients at site 1 and the straining coefficient at site 2 are responsible for the retention of $nSiO_2$ with HA in porous sand media. Owing to numerous complex substances in the soil and underground water system, further work will be required on the transport of $nSiO_2$ in soil to better understand the transport behaviors of $nSiO_2$. Overall, the information presented herein may be useful for assessing the environmental exposure and risk of $nSiO_2$ in natural system with the enrichment of HA and for eventually developing regulations for such ENMs.

Acknowledgments We also greatly appreciate the support from the Jiangsu Collaborative Innovation Center of Technology and Material for Water Treatment.

Funding information This research was funded by the National Natural Science Foundation of China (grant nos. 21777110 and 21377090).

References

Adams LK, Lyon DY, Alvarez PJ (2006) Comparative eco-toxicity of nanoscale TiO_2, SiO_2, and ZnO water suspensions. Water Res 40(19):3527–3532

Amirbahman A, Olson TM (1995) Deposition kinetics of humic matter-coated hematite in porous media in the presence of Ca^{2+}. Colloids Surf A Physicochem Eng Asp 99(1):1–10

Bayat AE, Junin R, Shamshirband S, Chong WD (2015) Transport and retention of engineered Al_2O_3, TiO_2, and SiO_2 nanoparticles through various sedimentary rocks. Sci Rep 5(1):1–12

Ben-Moshe T, Dror I, Berkowitz B (2010) Transport of metal oxide nanoparticles in saturated porous media. Chemosphere 81(3):387–393

Bolster CH, Mills AL, Hornberger GM, Herman JS (1999) Spatial distribution of deposited bacteria following miscible displacement experiments in intact cores. Water Resour Res 35(6):1797–1807

Bradford SA, Simunek J, Bettahar M, van Genuchten MT, Yates SR (2003) Modeling colloid attachment, straining, and exclusion in saturated porous media. Environ Sci Technol 37(10):2242–2250

Bradford SA, Kim HN, Haznedaroglu BZ, Torkzaban S, Walker SL (2009) Coupled factors influencing concentration-dependent colloid transport and retention in saturated porous media. Environ Sci Technol 43(18):6996–7002

Chen G, Liu X, Su C (2012) Distinct effects of humic acid on transport and retention of TiO_2 rutile nanoparticles in saturated sand columns. Environ Sci Technol 46(13):7142–7150

Chen M, Xu N, Cao X, Zhou K, Chen Z (2015) Facilitated transport of anatase titanium dioxides nanoparticles in the presence of phosphate in saturated sands. J Colloid Interface Sci 451:134–143

Chen M, Xu N, Christodoulatos C, Wang D (2018) Synergistic effects of phosphorus and humic acid on the transport of anatase titanium dioxide nanoparticles in water-saturated porous media. Environ Pollut 243:1368–1375

Cho JW, Sul KI (2001) Characterization and properties of hybrid composites prepared from poly (vinylidene fluoride–tetrafluoroethylene) and SiO_2. Polymer 42(2):727–736

Cho M, Cho WS, Choi M, Kim SJ, Han BS, Kim SH, Kim HO, Sheen YY, Jeong J (2009) The impact of size on tissue distribution and elimination by single intravenous injection of silica nanoparticles. Toxicol Lett 189:177–183

Chowdhury I, Cwiertny DM, Walker SL (2012) Combined factors influencing the aggregation and deposition of nano-TiO_2 in the presence of humic acid and bacteria. Environ Sci Technol 46(13):6968–6976

Cochrane H, Lin CS (1993) The influence of fumed silica properties on the processing, curing, and reinforcement properties of silicone rubber. Rubber Chem Technol 66(1):48–60

Diener L, Wick P, Kaiser JP (2013) Nanoparticles in paints: A new strategy to protect façades and surfaces? J Phys Conf Ser 429:12036–12045

Doshi R, Braida W, Christodoulatos C, Wazne M, Gregory O (2008) Nano-aluminum: transport through sand columns and environmental effects on plants and soil communities. Environ Res 106(3):296–303

Esfahani A, Firouzi A, Sayyad G, Kiasat A (2014) Transport and retention of polymer-stabilized zero-valent iron nanoparticles in saturated porous media: effects of initial particle concentration and ionic strength. J Ind Eng Chem 20(5):2671–2679

Espinasse B, Hotze EM, Wiesner MR (2007) Transport and retention of colloidal aggregates of C_{60} in porous media: effects of organic macromolecules, ionic composition, and preparation method. Environ Sci Technol 41(21):7396–7402

Fisher-Power L, Cheng T (2018) Nanoscale titanium dioxide ($nTiO_2$) transport in natural sediments: importance of soil organic matter and Fe/Al oxyhydroxides. Environ Sci Technol 52(5):2668–2676

Fruijtier-Polloth C (2012) The toxicological mode of action and the safety of synthetic amorphous silica—a nanostructured material. Toxicology 294(2–3):61–79

Guggenberger G, Rodionov A, Shibistova O, Grabe M, Kasansky OA, Fuchs H, Mikheyeva N, Zrazhevskaya G, Flessa H (2008) Storage and mobility of black carbon in permafrost soils of the forest tundra ecotonein Northern Siberia. Glob Chang Biol 14(6):1367–1381

Hahn MW, O'meliae CR (2004) Deposition and reentrainment of brownian particles in porous media under unfavorable chemical conditions: some concepts and applications. Environ Sci Technol 38(1):210–220

Jiang X, Tong M, Li H, Yang K (2010) Deposition kinetics of zinc oxide nanoparticles on natural organic matter coated silica surfaces. J Colloid Interface Sci 350(2):427–434

Johnson PR, Elimelech M (1995) Dynamics of colloid deposition in porous media: blocking based on random sequential adsorption. Langmuir 11(3):801–812

Johnson RL, Johnsinm GO, Nurmi JT, Tratnyek PG (2009) Natural organic matter enhanced mobility of nano zerovalent iron. Environ Sci Technol 43(14):5455–5460

Jung B, O'Carroll D, Sleep B (2014) The influence of humic acid and clay content on the transport of polymer-coated iron nanoparticles through sand. Sci Total Environ 496:155–164

Kretzschmar R, Borkovec M, Grolimund D, Elimelech M (1999) Mobile subsurface colloids and their role in contaminant transport. Adv Agron 66(08):121–193

Li Z, Barnes JC, Bosoy A, Stoddart JF, Zink JI (2012) Cheminform abstract: mesoporous silica nanoparticles in biomedical applications. Chem Soc Rev 41(7):2590–2605

Liang Y, Bradford S, Simunek J, Heggen M, Vereecken H, Klumpp E (2013) Retention and remobilization of stabilized silver nanoparticles in an undisturbed loamy sand soil. Environ Sci Technol 47(21):12229–12237

Liu X, Wazne M, Chou T, Xiao R, Xu S (2011) Influence of Ca^{2+} and Suwannee River Humic Acid on aggregation of silicon nanoparticles in aqueous media. Water Res 45(1):105–112

Liu C, Xu N, Feng G, Zhou D, Cheng X, Li Z (2017) Hydrochars and phosphate enhancing the transport of nanoparticle silica in saturated sands. Chemosphere 189:213–223

Loon CK, Menachem E (2008) Interaction of fullerene (C_{60}) nanoparticles with humic acid and alginate coated silica surfaces: measurements, mechanisms, and environmental implications. Environl Sci Technol 42(20):7607–7614

Napierska D, Thomassen LC, Lison D, Martens JA, Hoet PH (2010) The nanosilica hazard: another variable entity. Part Fibre Toxicol 7:39–70

Nel A, Xia T, Mädler L, Li N (2006) Toxic potential of materials at the nanolevel. Science 311(5761):622–627

Oberdörster G, Ferin J, Lehnert BE (1994) Correlation between particle size, in vivo particle persistence, and lung injury. Environ Health Perspect 102(suppl 5):173–179

Redman JA, Grant SB, Olson TM, Estes MK (2001) Pathogen filtration, heterogeneity, and the potable reuse of wastewater. Environ Sci Technol 35(9):1798–1805

Redman AD, Macalady DL, Ahmann D (2002) Natural organic matter affects arsenic speciation and sorption onto hematite. Environ Sci Technol 36(13):2889–2896

Schijven JF, ŠimŮnek J (2002) Kinetic modeling of virus transport at the field scale. J Contam Hydrol 55(1–2):113–135

Schulman JH (1960) Colloid chemistry. Annu Rev Phys Chem 11(1):169–186

Simunek J, van Genuchten MT, Sejna M (2016) Recent developments and applications of the HYDRUS computer software packages. Vadose Zone J 15(7). https://doi.org/10.2136/vzj2016.04.0033

Solovitch N, Labille J, Rose J, Chaurand P, Borchneck D, Wiecner MR, Bottero JY (2010) Concurrent aggregation and deposition of TiO_2 nanoparticles in a sandy porous media. Environ Sci Technol 44(13):4897–4902

Svecova L, Cremel S, Sirguey C, Simonnot MO (2008) Comparison between batch and column experiments to determine the surface charge properties of rutile TiO_2 powder. J Colloid Interface Sci 325(2):363–370

Toloni I, Lehmann F, Ackerer P (2014) Modeling the effects of water velocity on TiO_2 nanoparticles transport in saturated porous media. J Contam Hydrol 171:42–48

Tufenkji N, Elimelech M (2005) Breakdown of colloid filtration theory: role of the secondary energy minimum and surface charge heterogeneities. Langmuir 21(3):841–852

USEPA (2007) Nanotechnology white paper. Prepared for the U.S. Environmental Protection Agency by members of the nanotechnology workgroup, a group of EPA's science policy council science policy council. U.S. Environmental Protection Agency, Washington, DC

Wang C, Bobba AD, Attinti R, Lazouskaya V, Wang LP, Jin Y (2012a) Retention and transport of silica nanoparticles in saturated porous media: effect of concentration and particle size. Environ Sci Technol 46(13):7151–7158

Wang D, Bradford SA, Harvey RW, Gao B, Cang L, Zhou D (2012b) Humic acid facilitates the transport of ARS-labeled hydroxyapatite nanoparticles in iron oxyhydroxide-coated sand. Environ Sci Technol 46(5):2738–2745

Wang D, Zhang W, Zhou D (2013) Antagonistic effects of humic acid and iron oxyhydroxide grain-coating on biochar nanoparticle transport in saturated sand. Environ Sci Technol 47(10):5154–5161

Xu X, Xu N, Cheng X, Guo P, Chen Z, Wang D (2017) Transport and aggregation of rutile titanium dioxide nanoparticles in saturated porous media in the presence of ammonium. Chemosphere 169:9–17

Xu N, Cheng X, Zhou K, Xu X, Li Z, Chen J (2018) Facilitated transport of titanium dioxide nanoparticles via hydrochars in the presence of ammonium in saturated sands: effects of pH, ionic strength, and ionic composition. Sci Total Environ 612:1348–1357

Yuan J, Xing W, Gu G, Wu L (2008) The properties of organic pigment encapsulated with nano-silica via layer-by-layer assembly technique. Dyes Pigments 76(2):463–469

Zhang W, Morales VL, Cakmak ME, Salvucci AE, Geohring LD, Hay AG, Parlange JY, Steenhuis TS (2010) Colloid transport and retention in unsaturated porous media: effect of colloid input concentration. Environ Sci Technol 44(13):4965–4972

Zhu Z, Andelman T, Yin M, Chen T, Ehrlich S, O'Brien S (2005) Synchrotron x-ray scattering of Zno nanorods: periodic ordering and lattice size. J Mater Res 20(4):1033–1041